

# On the Packing–Holding Flow in the Injection Molding of Thermoplastic Polymers

G. TITOMANLIO\* and S. PICCAROLO, *Istituto di Ingegneria Chimica, Università di Palermo, 90128 Palermo, Italy*, and  
G. LEVATI,<sup>†</sup> *Tecnopolimeri, Ceriano Laghetto (MI), Italy*

## Synopsis

Injection molding tests were performed on a Ny66 resin. Data of mass entering the mold during the packing–holding stage as a function of filling flow rate and holding time are presented. The experimental results are discussed on the basis of a simple model of the packing–holding stage. Only a small part of density increase due to crystallization seems to be compensated by the packing–holding extra flow.

## INTRODUCTION

The injection molding cycle may be decomposed into three stages: filling, packing–holding, and cooling. During filling hot polymer melt is forced into an empty cold cavity; once the cavity is filled, extra material is packed inside the cavity which is held under high pressure in order to compensate for density increase during cooling. The cooling stage starts when the cavity gate is sealed by polymer solidification; further temperature decrease and polymer crystallization takes place during the cooling stage and gives rise to pressure decrease inside the cavity.

So far most of researchers attention has been focused on the analysis of the filling stage, especially to the prediction of injection pressure and of flow front progression in complex molds. The fountain (or vulcano) flow at the melt front was also deeply analyzed gaining information on the phenomena which give rise to the microstructure at the surface of the finished article.

On the other hand, it is widely recognized that the microstructure beyond the skin of the final article, and thus its properties and quality, are determined by the packing–holding pressure and time. In particular, photoelasticity stress patterns,<sup>1</sup> birefringence, cooling stresses, density distributions, and product shrinkage<sup>2–4</sup> have been found to be tightly related to the packing–holding variables, which regulate the extra mass entering the cavity after filling.

Spencer and Gilmore<sup>5</sup> suggested an equation for the maximum pressure inside the molds during the packing–holding stage. Kamal and Kenig<sup>6</sup> assumed that the extra material flowing into the cavity during the packing–holding stage may be considered proportional to the difference between the injection pressure and the average pressure in the cavity. Later on, Kamal

\*To whom correspondence should be addressed.

<sup>†</sup> Present address: CESAP, Centro Europeo Sviluppo Applicaz Plastiche, Zogno (Bg), Italy

et al.<sup>7,8</sup> extended the Hele–Shaw analysis<sup>9</sup> to the packing stage for rectangular geometry; a linearized analytical expression for pressure distribution was obtained, accounting for viscosity changes across cavity thickness. The complete equations were solved numerically for various boundary conditions.<sup>10–12</sup>

More recently,<sup>13,14</sup> a much more detailed analysis was performed, solving numerically a set of differential equations where many of the relevant phenomena taking place during packing were accounted for locally with reference to a rectangular mold. In particular, the local crystallization rate was described by a nonisothermal modification<sup>15</sup> of the Avrami equation. Viscoelasticity was described by the Maxwell–Oldroyd–Gupta–Metzner equation, a shift factor on both viscosity and relaxation time being adopted to take care of temperature changes. Such an analysis includes most, if not all, available basic knowledge of the phenomena involved. Much insight, however, still needs to be gained also about the interactions between the different phenomena, such as the effect of crystal nucleation on rheology or density changes under simultaneous variations of pressure, temperature, and crystallinity. Before these matters will be further clarified, the informations gained from simpler models of polymer processing operations is still valuable and of useful reference to the development of more detailed simulation.

In this paper an attempt was made to describe the packing–holding stage on the basis of an extension<sup>16</sup> of Lord and Williams' analysis of mold filling.<sup>17</sup> The complete temperature field is considered, and a viscous non-Newtonian rheological equation is adopted. Crystallization is not explicitly accounted for in the energy equation mainly because kinetic information for nonisothermal processes is not sufficient for most polymers, particularly for nylon resins which were adopted in the experimental part of this work. The reduction of cooling rate by effect of crystallization heat release was, however, approximately accounted for by means of a suitable reduction of thermal diffusivity as described in Ref. 18. The model has to be solved numerically and is tailored to simple molds; more complex situations can, however, be analyzed by basic unit compositions. Experimental results regarding relevant aspects such as the extra material entering the mold during packing–holding are also presented and discussed with reference to the model predictions.

## EXPERIMENTAL

A nylon 66 injection molding grade, manufactured by SNIA-Tecnopolimeri commercially known as SNIAMID SSD AP/ST was adopted in this work. The same resin was used in a previous work for mold filling experiments.<sup>18</sup> Shear viscosity curves determined by capillary rheometers at several temperatures are well described by an equation of the following form:

$$\eta(\dot{\gamma}, T) = \frac{\eta_0(T)}{1 + C[\eta_0(T)\dot{\gamma}]^{1-n}} \quad (1)$$

$$\eta_0(T) = A \exp(b/T) \quad (2)$$

where  $\eta_0$  is zero shear rate viscosity and  $b$ ,  $n$ ,  $A$ , and  $C$  are material constants. Their values and other physical properties are reported in table I, further information is given in Ref. 18.

A Sandretto-7/95 reciprocating screw injection molding machine was adopted for the injection molding experiments. The screw diameter was 45 mm, the clamp force was 930 kN, and the injection machine was controlled by a microprocessor unit, control was based on the hydraulic system pressure. The material was injected in a disk shaped cavity 20 cm in diameter. The thickness was adjusted to decrease linearly with the radius from 0.36 cm at the center gate to 0.06 cm at the maximum disk diameter. The sprue was 6.5 cm long and tapered from a diameter of 0.4–0.8 cm at the cavity entrance. Pressure transducers were mounted in positions having radius  $r_t = 4.3$  and 6 cm. The injection machine was always operated holding constant the melt flow rate during the filling stage at each test; the flow rate was varied within the range 30–90 cm<sup>3</sup>/s. The barrel temperature was held at 290°C, and the mold was conditioned at 60°C for all tests. Results will be reported for tests performed with packing pressure and holding time  $t_n$  of 200 atms and 15 s, respectively.

The pressure at the transducer positions and the screw displacement were recorded during both filling and packing–holding stages. Typical pressure  $P$  and screw displacement  $d$  recordings are shown in Figure 1. In some cases a sharp maximum (dotted line in Fig. 1) was observed in the pressure curve soon after the estimated end of filling stage. In those cases the screw displacement  $d$  also showed a parallel small maximum. This feature was ascribed to the inertia of the injecting system which, after commutation to the packing

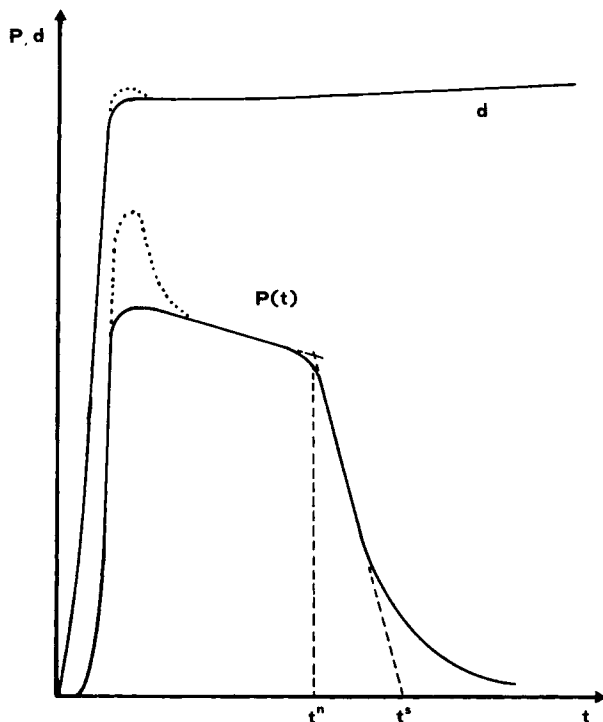


Fig. 1. Typical experimental recordings.  $d$  is screw displacement;  $P$  is pressure inside the cavity.

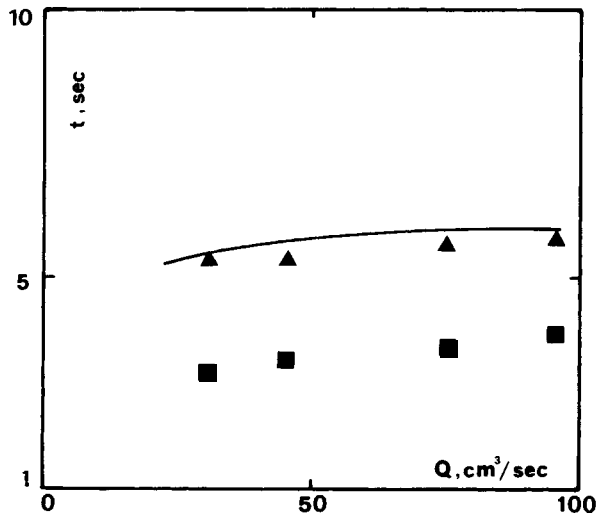


Fig. 2. Values of  $t^n$  (▲) and  $t^n$  (■) as a function of filling flow rate (obtained as shown in Fig. 1 from experimental recordings at a transducer radial position of 6 cm). Model predictions are evaluated adopting  $x_s = 0.05$  (—) as solidification criterion.

pressure, depending on conditions, can give rise to a pressure pulse within the cavity. For other values of the injection rate and packing pressure, the maximum in the cavity pressure curve (full line in Fig. 1) was flat; similarly the screw displacement resulted monotonously increasing with time  $t$ .

After the maximum, the pressure decrease was closely linear up to an instant,  $t^n$  in Figure 1, where a sharp slope increase was observed. Smaller

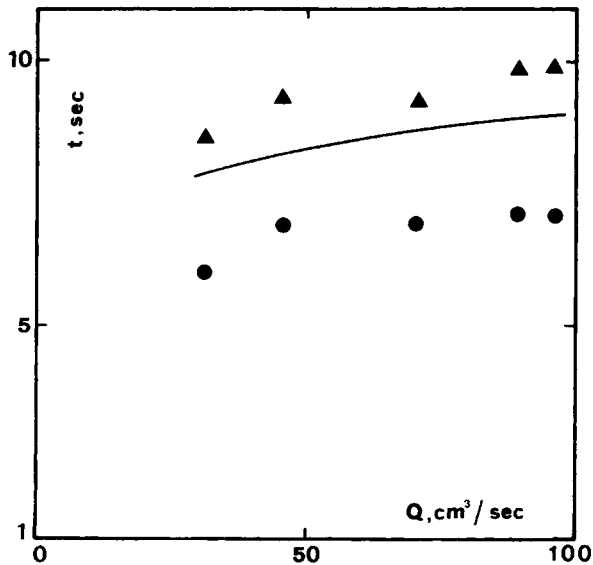


Fig. 3. Values of  $t^n$  (▲) and  $t^n$  (●) as a function of filling flow rate (obtained as shown in Fig. 1 from experimental recordings at a transducer radial position of 4.3 cm). Model predictions are evaluated adopting  $x_s = 0.05$  (—) as solidification criterion.

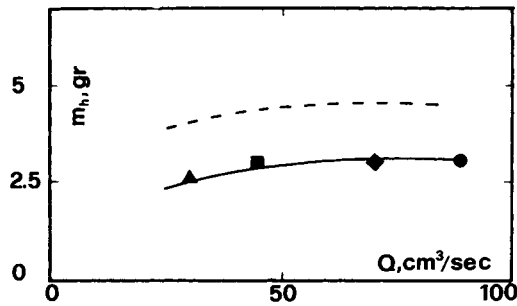


Fig. 4. Mass  $m_h$  entering the mold during holding vs. filling flow rate  $Q$ .  $X_s$ : (---) 0.2; (—) 0.05.

values of  $t^n$  were observed at the larger radial transducer position. In all tests the pressure decrease that resulted was linear also for a short time interval after  $t^n$ ; afterwards the curve slope decreased gradually toward zero. Also the time  $t^s$  obtained by extrapolating down to zero pressure the linear behavior subsequent to  $t^n$  is identified in Figure 1. Both time values,  $t^n$  and  $t^s$  are plotted as a function of the filling flow rate  $Q$  in Figures 2 and 3 for transducer positions  $r_t = 6$  and 4.3 cm, respectively.

The first pressure decrease up to  $t^n$  may be due to both the growth of the solid layer thickness next to the mold walls and the effect of temperature on viscosity upstream to the transducer positions; both of them indeed give rise to an increase of pressure drop related to the packing-holding extra flow. The sharpness of the slope increase in the pressure curves at  $t^n$  is an indication of the onset of a new phenomenon which controls the pressure drop after  $t^n$ . The subsequent gradual decrease of the pressure toward a constant value is an indication of the achievement of a solid state at the transducer positions.

Results of mass entering the mold  $m_h$  after 15 s holding were obtained from screw displacements data. These are shown in Figure 4 vs. filling flow rate. Some transient results for  $m(t)$  are considered in Figure 5 where  $m_h - m(t)$  is plotted vs.  $t_h - t$ ; these coordinates were chosen to better show details at long times when  $t$  gets close to  $t_h$ .

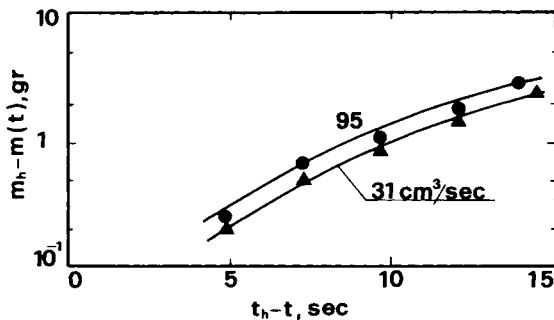


Fig. 5. Transient results for mass  $m(t)$  entering the cavity during holding.  $m_h$  is the mass entering the cavity during the overall holding time  $t_h$ . Lines are predictions for  $x_s = 0.05$ .  $Q$  ( $\text{cm}^3/\text{s}$ ): (●) 95; (▲) 31.

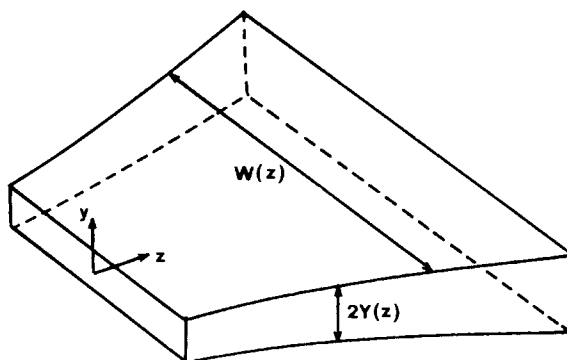


Fig. 6. Scheme of a rectangular channel of variable width  $W(z)$  and thickness  $2Y(z)$ .  $z$  is main flow direction.

### GOVERNING EQUATIONS

Lord and Williams' analysis for mold filling<sup>17</sup> is here extended to the packing–holding stage of the injection molding process. The main difference between filling and packing is related to the role played by density changes taking place in the polymer because of temperature, pressure, and crystallinity variations. These indeed give rise to negligible contribution to the filling flow rate and vice versa are the true driving force for the extra flow taking place during packing and holding.

A channel having variable width  $W(z)$  and thickness  $2Y(z)$ ,  $z$  being the main flow direction, is shown in Figure 6. With reference to this geometry, in each section normal to the main flow direction, the packing flow rate  $M(z, t)$  is determined by the density increase downstream to  $z$  and upstream to the first completely solidified section  $z_s$  where flow rate is zero.

One can thus write

$$M(z, t) = 2 \int_z^{z_s} W(z) \int_0^{Y(z)} \frac{\partial \rho(T, P, x_c)}{\partial t} dy dz \quad (3)$$

Usually  $M(z, t)$  is positive; however, pressure and temperature distributions may combine so as to give rise to a negative flow rate through some sections within the mold.

The identification of completely solidified sections is not straightforward. A general definition of solidified section should be related to the value of the dominant relaxation time in the midplane (where solidification is reached later in each cross section): When relaxation time is sufficiently larger than the process characteristic time, the material has to be considered solid. Unfortunately, material rheology under simultaneous temperature decrease and crystallization increase is not sufficiently investigated, and any estimate of relaxation time under these conditions is not reliable. Introducing crystallization kinetic in the model would thus be of little help at least as far as the evaluation of  $z_s$  is concerned.

Crystallization kinetic is thus ignored in the energy equation, however, the cooling rate decrease by effect of crystallization heat release is estimated by modifying thermal diffusivity as described in Ref. 18. Furthermore, as specified

TABLE I  
 List of Dimensionless Variables<sup>a</sup>

Channel having variable thickness		Tube having variable radius $R(z)$	
$\mathbf{y} = \frac{y}{Y(z)}$ ;	$\mathbf{z} = \frac{z}{Y_0}$	$\mathbf{r} = \frac{r}{R(z)}$ ;	$\mathbf{z} = \frac{z}{R_0}$
$\mathbf{u} = \frac{Y_0 u}{\alpha}$ ;	$\mathbf{t} = \frac{\alpha t}{Y_0^2}$	$\mathbf{u} = \frac{R_0 u}{\alpha}$ ;	$\mathbf{t} = \frac{\alpha t}{R_0^2}$
$\mathbf{P} = \frac{PY_0^2}{A\alpha}$ ;	$\mathbf{M} = \frac{M}{2W_0\alpha\rho_1}$	$\mathbf{P} = \frac{PR_0^2}{A\alpha}$ ;	$\mathbf{M} = \frac{M}{2\pi\alpha\rho_1 R_0}$
$\mathbf{B} = \frac{A\alpha}{Y_0^2 k \Delta T}$ ;	$\mathbf{F} = \frac{C^{1/(1-n)} A \alpha}{Y_0^2}$	$\mathbf{B} = \frac{A\alpha}{R_0^2 k \Delta T}$ ;	$\mathbf{F} = \frac{C^{1/(1-n)} A \alpha}{R_0^2}$
$\mathbf{T} = \frac{T - T_w}{T_i - T_w}$ ;	$\mathbf{H} = \frac{T_w}{T_i - T_w}$ ;	$\mathbf{V} = \frac{b - T_w}{T_i - T_w}$	
$\eta = \frac{\eta}{A}$ ;	$\rho = \frac{\rho}{\rho_1}$ ;	$\Delta T = T_i - T_w$	

<sup>a</sup>Bold face characters are adopted for dimensionless quantities.

below, a solidification criterion based on temperature (rather than on relaxation time) is adopted.

Energy and momentum balance equations are similar to those describing the filling stage,<sup>18</sup> the only difference being a flow rate  $M$  not constant over the mold but rather variable so as described by eq. (3). The balance and rheological equations are listed below in dimensionless form with reference to the geometry of Figure 6. The definition of dimensionless variables is given in Table I. Neglecting longitudinal conduction and transverse convection, the energy equation becomes

$$\frac{\partial \mathbf{T}}{\partial \mathbf{t}} + \mathbf{u} \frac{\partial \mathbf{T}}{\partial \mathbf{z}} = \left[ \frac{Y_0}{Y(z)} \right]^2 \frac{\partial^2 \mathbf{T}}{\partial \mathbf{y}^2} + \mathbf{B} \mathbf{y} \frac{\partial \mathbf{P}}{\partial \mathbf{z}} \frac{\partial \mathbf{u}}{\partial \mathbf{y}} \quad (4)$$

with boundary conditions

$$\frac{\partial \mathbf{T}}{\partial \mathbf{y}}(\mathbf{t}, \mathbf{z}, 0) = 0, \quad \text{symmetry} \quad (5)$$

$$\mathbf{T}(\mathbf{t}, 0, 1) = 1, \quad \text{inlet temperature} \quad (6)$$

$$\mathbf{Y}(\mathbf{t}, \mathbf{z}, 1) = 0, \quad \text{wall temperature} \quad (7)$$

The initial temperature field is that determined at the end of filling stage.

Under lubrication approximation the momentum balance can be written as

$$\mathbf{u} = - \frac{d\mathbf{P}}{d\mathbf{z}} \left[ \frac{Y(z)}{Y_0} \right]^2 \int_{\mathbf{y}}^1 \frac{\mathbf{y}}{\eta} d\mathbf{y} \quad (8)$$

TABLE II  
Governing Equations for a Tube Having Variable Radius  $R(z)$

$$\mathbf{M}(x, t) = \left[ \frac{R(z)}{R_0} \right]^2 \int_0^1 \rho \mathbf{u} r dr = \int_{L/R_0}^{z/R_0} \left[ \frac{R(z)}{R_0} \right]^2 \int_0^1 \frac{\partial \rho}{\partial t} r dr dz$$

$$\mathbf{u} = -\frac{1}{2} \frac{\partial \mathbf{P}}{\partial \mathbf{z}} \left[ \frac{R(z)}{R_0} \right]^2 \int_r^1 \frac{r}{\eta} dr$$

$$\frac{\partial \mathbf{T}}{\partial t} + \mathbf{u} \frac{\partial \mathbf{T}}{\partial \mathbf{z}} = \left[ \frac{R_0}{R(z)} \right]^2 \frac{1}{r} \frac{\partial}{\partial r} \left( r \frac{\partial \mathbf{T}}{\partial r} \right) + \mathbf{B} \frac{r}{2} \frac{\partial \mathbf{P}}{\partial \mathbf{z}} \frac{\partial \mathbf{u}}{\partial r}$$

$$\eta = \eta_0 / \left\{ 1 + \left[ \mathbf{F} \eta_0 \frac{d\mathbf{u}}{dz} \frac{R_0}{R(z)} \right]^{1-n} \right\}$$

$$\eta_0 = \exp \left( \frac{\mathbf{V} + \mathbf{H}}{\mathbf{T} + \mathbf{H}} \right)$$

and continuity

$$\mathbf{M}(\mathbf{z}, t) = \frac{W(z)}{W_0} \frac{Y(z)}{Y_0} \int_0^1 \mathbf{u} \rho d\mathbf{y} = \int_{z/Y_0}^{z_s/Y_0} \frac{W(z)}{W_0} \frac{Y(z)}{Y_0} \int_0^1 \frac{\partial \rho}{\partial t} d\mathbf{y} dz \quad (9)$$

the initial value of  $z_s$ , being the mold length  $L$  along the main flow direction.

The dimensionless rheological equation becomes

$$\eta = \eta_0 / \left[ 1 + \left( \mathbf{F} \eta_0 \frac{d\mathbf{u}}{d\mathbf{y}} \frac{Y_0}{Y(z)} \right)^{1-n} \right] \quad (10)$$

where

$$\eta_0 = \exp \left( \frac{\mathbf{V} + \mathbf{H}}{\mathbf{T} + \mathbf{H}} \right)$$

Similar equations can be written for a tube having variable radius; they are listed in Table II.

A constitutive relation for density is needed in order to make the problem self-consistent. This relation was divided into three equations: one for the solid state, another for the melt state, and the third one for the transition region between the temperatures  $T_b$  and  $T_e$ , at which crystallization begins and ends, respectively. With the aim of a simple analysis which neglects crystallization kinetic, constant values were given to  $T_b$  and  $T_e$ . In particular, the values of  $T_b$  and  $T_e$  were chosen on the basis of results of differential scanning calorimetry tests performed at different cooling rates; their values are reported in Table III.

The effects of temperature and pressure on the polymer density above  $T_b$  and below  $T_e$  were simply described by thermal expansion and pressure coefficients combined according to the following equations:

$$\rho = [\rho_1 - \epsilon_1(T - T_1)] \exp[\beta_1(P - P_0)] \quad \text{for } T > T_b \quad (11)$$

$$\rho = [\rho_2 - \epsilon_2(T - T_2)] \exp[\beta_2(P - P_0)] \quad \text{for } T < T_e \quad (12)$$

where  $\rho_1$  and  $\rho_2$  are density values at both reference pressure  $P_0$  and temperatures  $T_1$  and  $T_2$ , respectively.



TABLE III  
Physical and Rheological Constants for Nylon 66

$b = 9430 \text{ K}$	$A = 2.2 \times 10^{-5} \text{ P}$	$C = 2.09 \times 10^{-7} \text{ g}/(\text{cm s})^{n-1}$
$n = 0.3$	$T_b = T_1 = 480 \text{ K}$	$T_e = T_2 = 450 \text{ K}$
$\epsilon_2 = 4 \times 10^{-4} \text{ g}/(\text{cm K})$		$\epsilon_1 = 4.4 \times 10^{-4} \text{ g}/(\text{cm K})$
$\beta_2 = 1.5 \times 10^{-5} \text{ atm}$		$\beta_1 = 4.5 \times 10^{-5} \text{ atm}$
$\rho_2 = 1.09 \text{ g}/\text{cm}^3$		$\rho_1 = 1.02 \text{ g}/\text{cm}^3$

The values  $T_b$  and  $T_e$  were taken as reference temperatures  $T_1$  and  $T_2$  for the melt and the solid, respectively. The densities  $\rho_i$  and the coefficients  $\epsilon_i$  and  $\beta_i$  are also given in Table I. Within the interval  $T_e - T_b$  the density was let to change linearly with temperature from the solid value at  $T_e$  to the melt value at  $T_b$ , both being evaluated at the actual pressure.

If crystallization kinetic equations and related data were available, they would allow a detailed description of density changes between  $T_b$  and  $T_e$ . The simple choice made for the density changes in the temperature interval  $T_e - T_b$  is consistent with a parallel simple scheme for crystallinity changes in the same temperature interval, i.e., a linear change of crystallinity with temperature in the interval  $T_e - T_b$ . Within this scheme, a solidification criterion based on temperature is equivalent to a solidification criterion based on crystallinity.

## DISCUSSION

The model equations were solved numerically according to the discretizing scheme outlined in Refs. 16 and 17. The simulation was extended to both sprue and cavity by composition of two units: a tube of variable radius for the sprue and a channel having width and thickness changing linearly along the main flow direction for the cavity. In order to use the same dimensionless time for both units, the reference lengths  $Y_0$  and  $R_0$  were taken equal to each other;  $Y(z)/Y_0$  and  $R(z)/R_0$  were calculated accordingly.

The contribution of the viscous heat generation was found to be irrelevant and that of convection resulted minor in the energy balance, obviously after the end of mold filling. The energy balance, during holding and cooling stages, remains thus essentially uncoupled from the other balance equations, and the thermal problem becomes essentially a conductive transient, starting from the temperature field existing at the end of the filling stage. Once viscous heat generation and convection were found to be negligible, the computational procedure outlined in Figure 7 was adopted.

Thermal diffusivity  $\alpha$  is the only thermal parameter which is left in the definition of dimensionless variables of Table I. It is smaller in the melt than in the solid polymer; furthermore, heat of crystallization slows down material cooling. The problem of an 'equivalent thermal diffusivity' in transient heat conduction through a transition temperature was previously considered.<sup>18,19</sup> In particular, some numerical results for the cooling time were reported as function of Stefan number for the ratios  $\mathbf{D} = K_s/K_m = 2$  and  $\mathbf{E} = \alpha_s/\alpha_m = 2.5$  of solid to melt thermal conductivities and diffusivities. These values of  $\mathbf{D}$  and  $\mathbf{E}$  are very close to those of Ny66 under the injection conditions adopted in

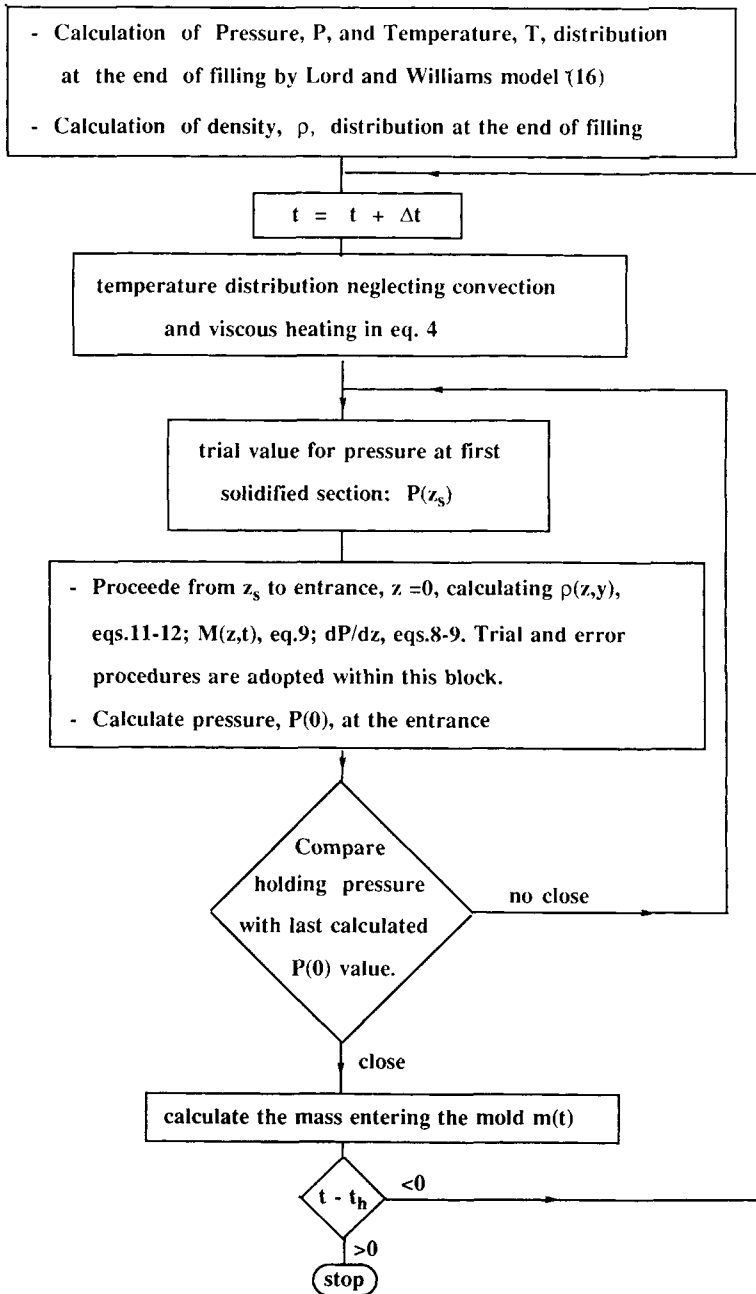


Fig. 7. Outline of computational procedure.

this work. The Stefan number was calculated here from the enthalpy of crystallization accounting for forty percent crystallinity. A value of  $4.5 \times 10^{-4} \text{ cm}^2/\text{s}$  was thus obtained for the "equivalent thermal diffusivity" with reference to the tests considered here.

The experimental results are compared in Figure 4 with model predictions for the extra mass entering the mold during 15 s holding. All physical

parameters adopted for the calculations are reported in Table III; for the solid properties, reference was made to 40% crystallinity. The section solidification criterion was based on the temperature at the section midplane. As mentioned in the previous section, rheology under both temperature decrease and crystallization increase is not investigated sufficiently to identify under which crystallinity index the material has to be considered solid. The value of the solidification index  $x_s$  thus has to be considered an adjustable parameter. The model predictions, reported in Figure 4, were evaluated for two values of  $x_s$ , 0.05 and 0.2, which correspond to two values of the solidification temperature  $T_s$  (i.e., 476 and 465 K). Predictions for  $x_s = 0.05$  are much closer to the experimental results. This indicates that soon after nucleation ends at the midplane, most of the packing flow stops in that section. A relevant part of density increase due to crystallization contributes, however, to the packing flow rate  $M$ . This is due to the fact that, at the instant of section solidification, crystallization index is 0.05 at the midplane and increases with the distance from the midplane, as also the temperature decreases with it. When packing flow stops, any further temperature decrease and/or crystallinity increase contributes only to cooling stresses or shrinkage build up.

Experimental results for the extra mass entering the mold during holding versus time are compared in Figure 5 with model predictions for  $x_s = 0.05$ , which was identified as best fitting value by the comparison in Figure 4. Only the largest and the smallest filling flow rate are there considered. The features shown by the data are closely reproduced by model predictions.

The values of time  $t^n$  and  $t^s$  obtained from the experimental pressure recordings are compared in Figures 2 and 3 with the model predictions for the time  $t_s$  to reach solidification temperature  $T_s = 476$  K, i.e., crystallinity index  $x_s = 0.05$ , at the midplane in the transducer positions. Model predictions for  $t_s$  are much closer to  $t^s$  than to  $t^n$ . The larger deviation between  $t_s$  and  $t^s$  is given in Figure 3, where model predictions for  $t_s$  are somewhat smaller, while in Figure 2 they are slightly larger than experimental  $t^s$  values. We only mention one possibility for such a slight deviation, that is, the wall boundary condition adopted to the energy equation: The mold wall temperature, instead of being constant, may increase somewhat with time, thus enlarging the experimental solidification time. This aspect becomes more important when longer times are involved as in the case of Figure 3 which relates to thicker sections. The fact that the solidification time  $t_s$  is much closer to  $t^s$  than to  $t^n$  suggests that the pressure decrease between  $t^n$  and  $t^s$  takes place under crystallinity values, at the section midplane, of only a few percent. If this is the case, the phenomenon related to the slope increase of the pressure curve between times  $t^n$  and  $t^s$  in Figure 1 has to be related to the viscosity increase by the effect of crystal nucleation and incipient crystallization.

### CONCLUDING REMARKS

The comparison reported in Figures 2-5 between experimental data and model predictions seems encouraging; however, it has to be pointed out that the value of solidification crystallization index  $x_s$  was treated as a fitting parameter.

When rheological description during solidification is available, a reliable and direct section solidification criterion can be identified. The calculation of extra

mass entering the mold during packing–holding stage could thus be carried out independently from the value of a fitting parameter. This would allow the estimate of residual density increase after cross section solidification, which in turn determines the shrinkage and cooling stresses build up in the finished article. Obviously a complete model has to account also for viscoelasticity and crystallization kinetics.

This work was carried out with financial support of CNR grant CT86.01582.03 and MPI.

### APPENDIX: NOMENCLATURE

<b>A</b>	constant in the rheological equation [see eq. (2)]
<b>b</b>	constant in the rheological equation [see eq. (2)]
<b>B</b>	Bridgman number (see Table II)
<b>C</b>	constant in the rheological equation [see eq. (1)]
<b>c</b>	specific heat
<b>d</b>	screw displacement
<b>D</b>	thermal conductivities ratio
<b>E</b>	thermal diffusivities ratio
<b>F</b>	dimensionless constant (see Table II)
<b>H</b>	dimensionless constant (see Table II)
<b>K</b>	thermal conductivity
$K_m$	melt thermal conductivity
$K_s$	solid thermal conductivity
<b>L</b>	mold length
$m_h$	mass entering the mold during holding
$m(t)$	mass entering the mold
<b>M</b>	mass flow rate
<b>M</b>	dimensionless mass flow (see Table II)
<b>n</b>	rheological constant [see eq. (1)]
<b>P</b>	pressure
$P(t)$	pressure at time $t$
<b>P</b>	dimensionless pressure (see Table II)
<b>Q</b>	filling flow rate
<b>r</b>	radius
<b>r</b>	dimensionless radius (see Table II)
$r_t$	transducer position
$R_0$	reference radius
$R(z)$	radius of a tube of variable section
<b>t</b>	time
<b>t</b>	dimensionless time (see Table I)
$t_h$	holding time
$t^n$	experimental time value (see Fig. 1)
$t^s$	experimental time value (see Fig. 1)
$t_s$	time to reach solidification temperature $T_s$ at section midplane
<b>T</b>	temperature
<b>T</b>	dimensionless temperature (see Table I)
$T_i$	inlet temperature
$T_s$	solidification temperature
$T_w$	wall temperature
$T_b$	temperature for incipient crystallization
$T_e$	temperature at end of crystallization
$T_1, T_2$	reference temperature [see eq. (11)]
<b>u</b>	primary velocity component
<b>u</b>	dimensionless velocity (see Table I)

$V$	dimensionless constant (see Table I)
$W(z)$	width of rectangular cavity
$x_c$	crystallinity index
$x_s$	crystallinity index at solidification temperature $T_s$
$y$	coordinate along the thickness direction
$y$	dimensionless coordinate in the thickness direction (see Table I)
$Y(z)$	half of channel thickness
$Y_0$	reference thickness
$z$	axial coordinate
$z$	dimensionless axial coordinate (see Table I)
$z_s$	axial coordinate of first completely solidified section
$\alpha$	thermal diffusivity
$\beta$	pressure expansion coefficient
$\epsilon$	thermal expansion coefficient
$\dot{\gamma}$	shear rate
$\eta$	viscosity
$\eta_0$	zero shear viscosity
$\eta$	dimensionless viscosity (see Table I)
$\eta_0$	dimensionless zero shear viscosity
$\rho$	density
$\rho$	dimensionless density

### Subscripts

- 1 refers to properties above  $T_1$
- 2 refers to properties below  $T_2$

### References

1. Y. T. Koita, *Polym. Eng. Sci.*, **14**, 840 (1974).
2. G. Menges, A. Dierkes, L. Schmidt, and E. Winkel, *SPE Tech. Pap.* **26**, 300 (1980).
3. A. Siegman, A. Buchman, and S. Kenig, *Polym. Eng. Sci.*, **22**, 40 (1982).
4. K. K. Wang, S. F. Shen, C. Cohen, C. A. Hieber, and A. I. Isayev, "Computer Aided Design and Fabrication of Molds and Control of Injection Molding", Tenth Prog. Rep., Cornell University, Ithaca, NY, Jan. 1984.
5. R. S. Spencer and R. D. Gilmore, *J. Colloid Sci.*, **6**, 118 (1951).
6. M. R. Kamal and S. Kenig, *Polym. Eng. Sci.*, **12**, 294, 302 (1972).
7. M. R. Kamal, Y. Kuo, and P. H. Doan, *Polym. Eng. Sci.*, **15**, 12 (1975).
8. Y. Kuo and M. R. Kamal, Proc. Int. Conf. Polym. Sci., Cambridge, MA, 1977.
9. H. Schlichting, *Boundary Layer Theory*, 6th ed., McGraw-Hill, New York, 1968, p. 114.
10. M. E. Ryan and T. S. Chung, *Polym. Eng. Sci.*, **20**, 642 (1980).
11. T. S. Chung and M. E. Ryan, *Polym. Eng. Sci.*, **21**, 271 (1981).
12. T. S. Chung, *Polym. Eng. Sci.*, **25**, 772 (1985).
13. M. R. Kamal and P. G. Lafleur, *Polym. Eng. Sci.*, **22**, 1069 (1982).
14. P. G. Lafleur and M. R. Kamal, *Polym. Eng. Sci.*, **26**, 92, 103 (1986).
15. K. Nakamura, T. Watanabe, K. Katayama, and T. Amano, *J. Appl. Polym. Sci.*, **16**, 1077 (1972).
16. G. Titomanlio, D. Acierno, and F. P. LaMantia, *Ing. Chim. Ital.*, **16**, 110 (1980).
17. H. A. Lord and G. Williams, *Polym. Eng. Sci.*, **15**, 569 (1975).
18. M. Virzi, G. Levati, and G. Titomanlio, *J. Polym. Mater.*, **4**, 103 (1987).
19. G. Titomanlio and S. Piccarolo, *Chem. Eng. Commun.*, **27**, 173 (1984).

Received October 14, 1986

Accepted July 27, 1987